Detailed Flow Measurements in a Centrifugal Compressor Vaneless Diffuser

A. Pinarbasi
Department of Mechanical Engineering,
University of Cumhuriyet,
Sivas, Turkey

M. W. Johnson
Department of Mechanical Engineering,
University of Liverpool,
Liverpool, United Kingdom

Hot-wire anemometer measurements have been made in the vaneless diffuser of a 1-m-dia low-speed backswept centrifugal compressor using a phase lock loop technique. Radial, tangential, and axial velocity measurements have been made on eight measurement planes through the diffuser. The flow field at the diffuser entry clearly shows the impeller jet-wake flow pattern and the blade wakes. The passage wake is located on the shroud side of the diffuser and mixes out slowly as the flow moves through the diffuser. The blade wakes, on the other hand, distort and mix out rapidly in the diffuser. Contours of turbulent kinetic energy are also presented on each of the measurement stations, from which the regions of turbulent mixing can be deduced.

Introduction

The overall efficiency of a centrifugal compressor is equally dependent on the good design of both impeller and diffuser. In the case of an impeller, the inlet flow is uniform; however, the diffuser must accept the outlet flow from the impeller, which is usually highly nonuniform with significant three-dimensional velocity components. The diffuser must remove these nonuniformities in velocity and flow direction while reducing the overall kinetic energy of the flow to produce a pressure recovery.

The flow at the exit of a centrifugal impeller has been measured by many authors (e.g., Eckardt, 1975; Johnson and Moore, 1983a, b; Krain, 1988). The flow invariably exhibits a jet-wake flow pattern, although the location of the wake position may be on the suction surface or the shroud depending on the impeller geometry and flow rate. The flow within vaneless diffusers has also been studied by many researchers (e.g., Inoue and Cumpsty, 1984; Maksoud and Johnson, 1987; Mounts and Brasz, 1992). These studies have shown how nonuniformities in the circumferential direction mix out rapidly, but those in the axial direction persist through the diffuser.

The objective of the current work was to repeat the work of Maksoud and Johnson (1987) but with a backswept impeller in place of their radial impeller. The resolution capability of the instrumentation system was also improved such that the number of points used on each measurement plane could be increased from less than 100 to around 700.

Experimental Procedure

Test Rig and Operating Condition. Experiments were carried out on the low-speed centrifugal compressor rig at the University of Liverpool. A schematic of the facility is shown in Fig. 1. The De Havilland Ghost impeller has been modified by replacing the original radial exit section of the blading by 30 deg backswept blading. The geometry of the original impeller is given by Johnson and Moore (1980) and that of the backswept blading in Fig. 2. The vaneless diffuser has straight walls and a constant cross-sectional area. The major geometric parameters, operating conditions, and measurement locations are given in Table 1.

Instrumentation and Measurement Technique

A constant-temperature hot-wire anemometer was used to measure the instantaneous velocity within the diffuser. Three wire orientations were used on three separate test runs to pro-

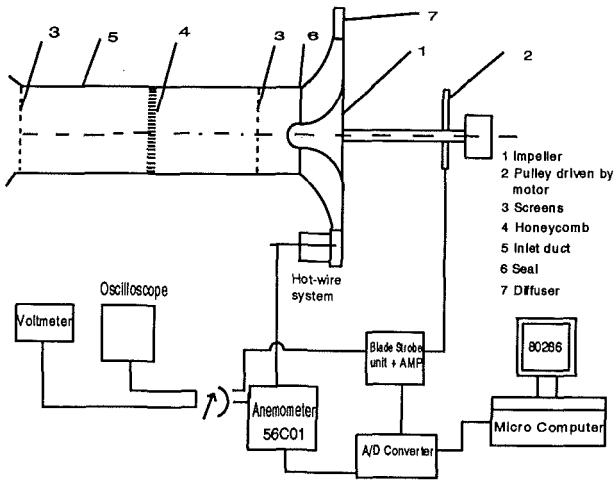


Fig. 1 Schematic of the test rig

Contributed by the International Gas Turbine Institute and presented at the 38th International Gas Turbine and Aeroengine Congress and Exposition, Cincinnati, Ohio, May 24–27, 1993. Manuscript received at ASME Headquarters February 19, 1993. Paper No. 93-GT-95. Associate Technical Editor: H. Lukas.

Copyright © 1994 by ASME
Downloaded 08 Mar 2011 to 193.140.144.9. Redistribution subject to ASME license or copyright; see http://www.asme.org/terms/Terms_Use.cfm

vide data from which the radial, axial, and tangential velocity components could be computed. A normal wire (Dantec 55P11) oriented in the circumferential direction was used during the first run and then a second wire set at 45 deg (Dantec 55P12) was used in its two possible orientations in the axial/radial plane, in the second and third runs. This choice of mutually perpendicular wire orientations ensured that the sign of the axial velocity component could be determined, which would not have been possible if the simplest orientation of wires in the circumferential, radial, and axial direction had been utilized. It was however necessary to assume that the radial velocity component was always positive and that the tangential velocity component was always in the direction of impeller rotation. The results showed that these assumptions were justified in that both velocity components maintained significant magnitudes at all measurement positions.

Hot-wire calibration was performed in two stages in a wind tunnel. First, a velocity/voltage calibration was performed for each wire with the wire perpendicular to the flow direction. A least rms error curve fitting technique to the King's law equation

$$E^2 = A + B \cdot U_e^c \tag{1}$$

was then employed to determine the calibration coefficients A, B, and C.

The second stage of calibration was necessary to determine the directional coefficients K and H to tangential and binormal velocity components. This was achieved by varying the wire

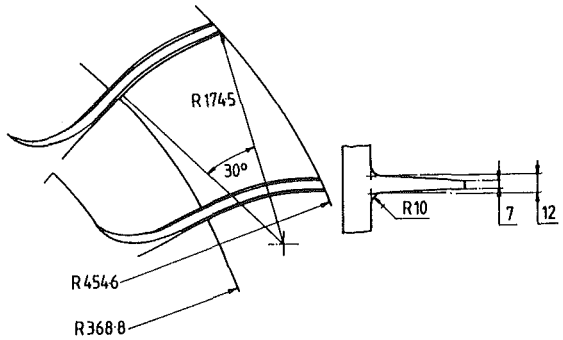


Fig. 2 Backswept blade geometry

Table 1 Geometry, operating condition, and measurement locations

Impeller Geometry and Operating Condition:

Inlet blade radius at the hub	R_h = 88.75 mm
Inlet blade radius at the shroud	R_s = 283.75 mm
Outlet radius	R_o = 454.6 mm
Backswept blade angle	β = 30°
Number of the blades	N = 19
Outlet blade span	b = 72.3 mm
Rotating speed	n = 500 rpm
Flowrate	Q = 0.142 kg/s

Measurement Locations:

Station	1	2	3	4	5	6	7	8
L/R_o	0.02	0.08	0.15	0.21	0.27	0.33	0.39	0.45

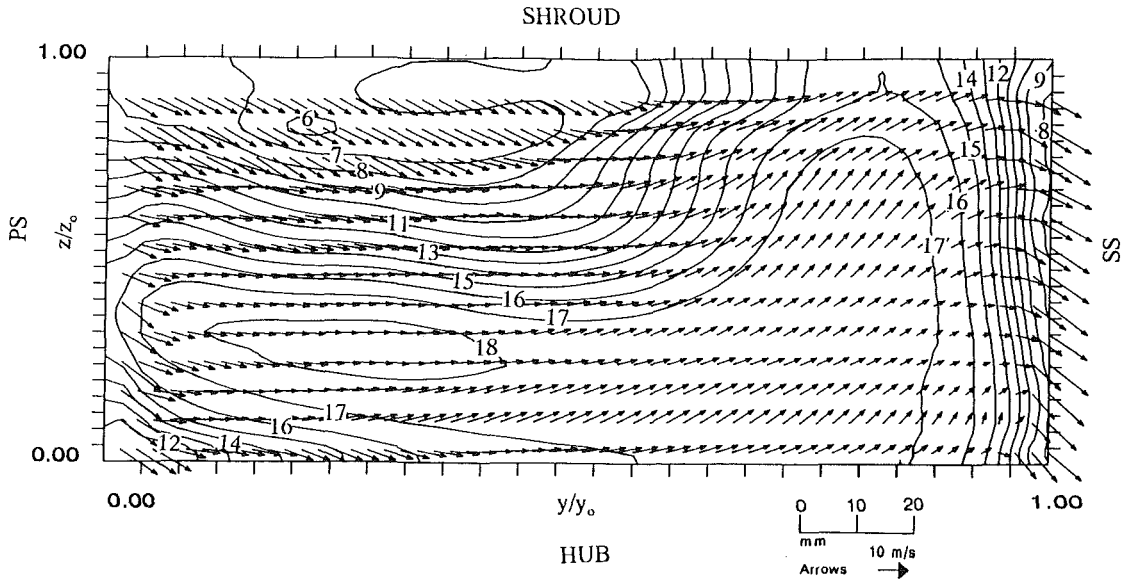


Fig. 3 Mean velocities at station 1 ($L/R_o = 0.02$)

Nomenclature

A, B, C = King's law calibration coefficients
E = hot-wire anemometer voltage
H, K = directional coefficients for hot wire
L = radial distance from impeller outlet
R_o = impeller outlet radius
U_e = effective cooling velocity
u_θ, u_r, u_z = tangential, radial, and axial mean velocity components
u_θ', u_r', u_z' = tangential, radial, and axial rms fluctuating velocity components
U_T = peripheral blade velocity at the impeller outlet
y/y_o = circumferential coordinate
z/z_o = axial coordinate

Downloaded 08 Mar 2011 to 193.140.144.9. Redistribution subject to ASME license or copyright; see http://www.asme.org/terms/Terms_Use.cfm

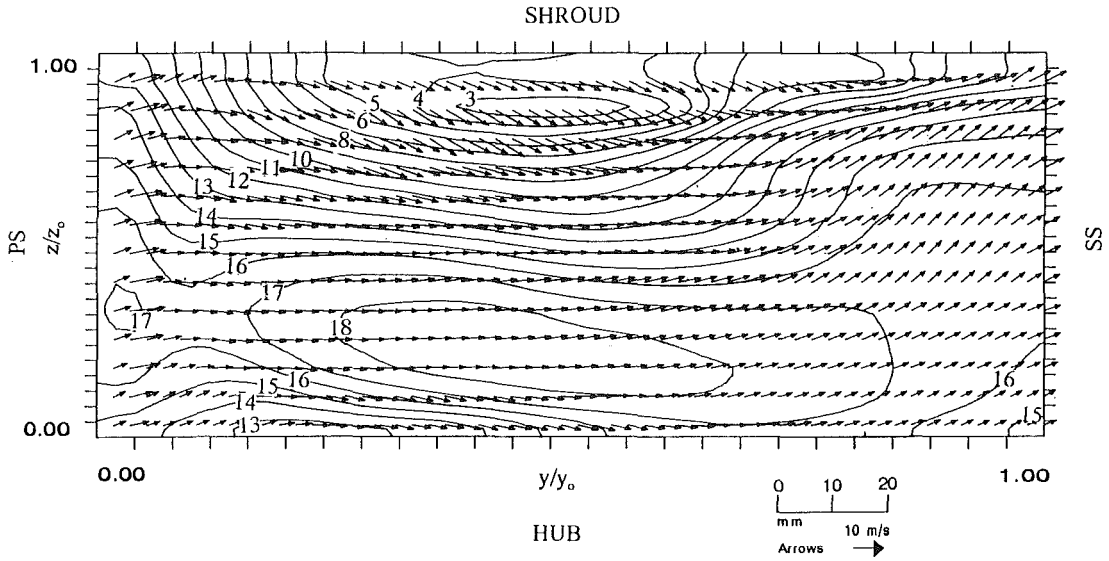


Fig. 4 Mean velocities at station 2 ($L/R_o = 0.08$)

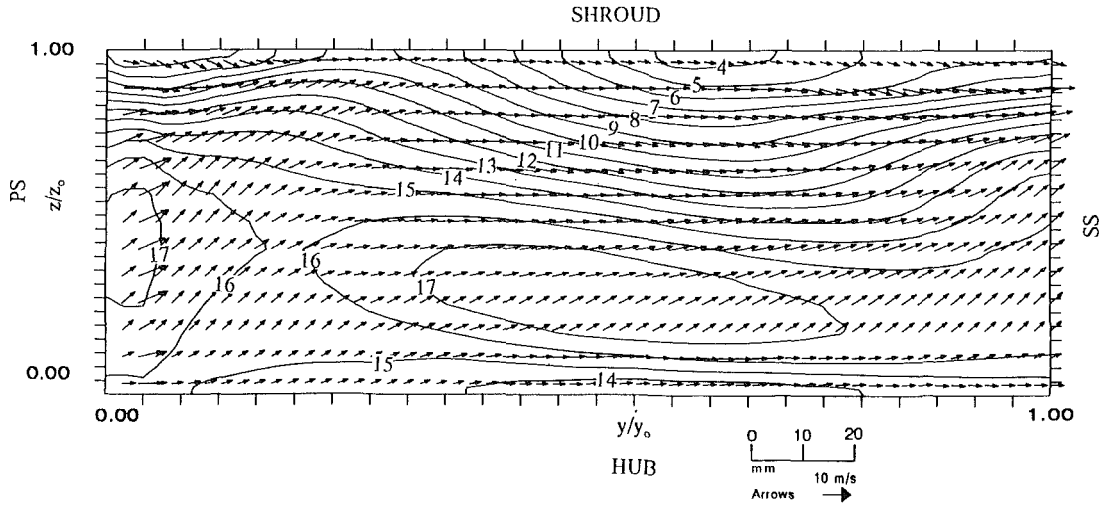


Fig. 5 Mean velocities at station 3 ($L/R_o = 0.15$)

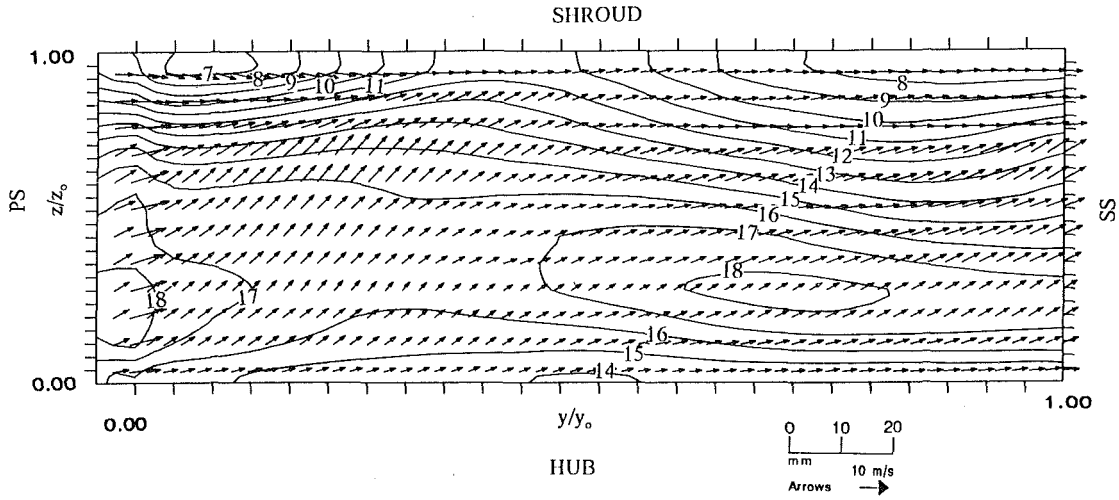


Fig. 6 Mean velocities at station 4 ($L/R_{oi} = 0.21$)

Downloaded 08 Mar 2011 to 193.140.144.9. Redistribution subject to ASME license or copyright; see http://www.asme.org/terms/Terms_Use.cfm

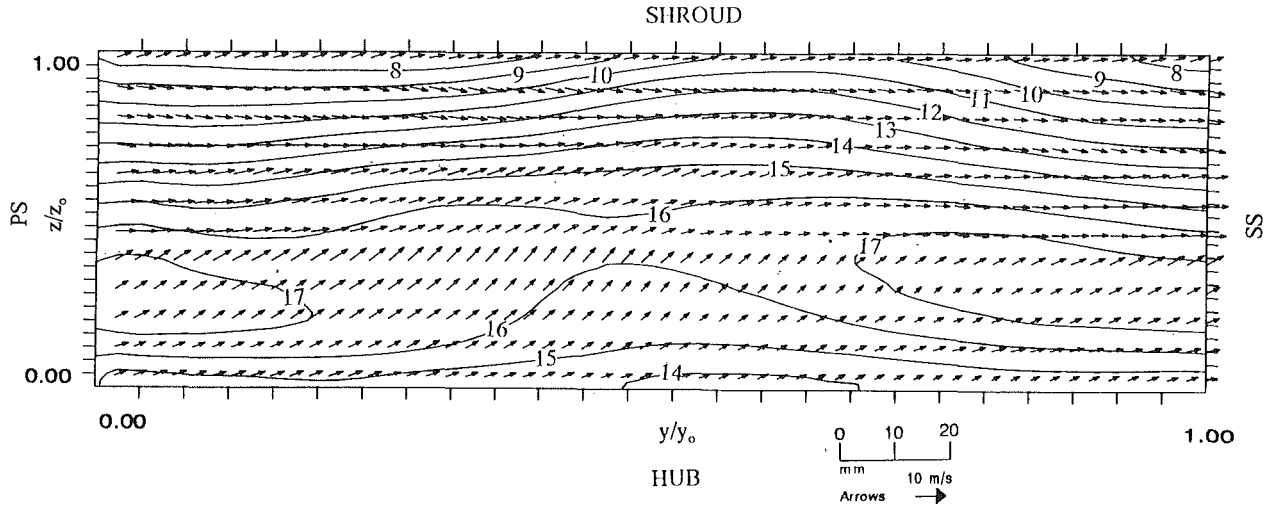


Fig. 7 Mean velocities at station 5 ($L/R_o = 0.27$)

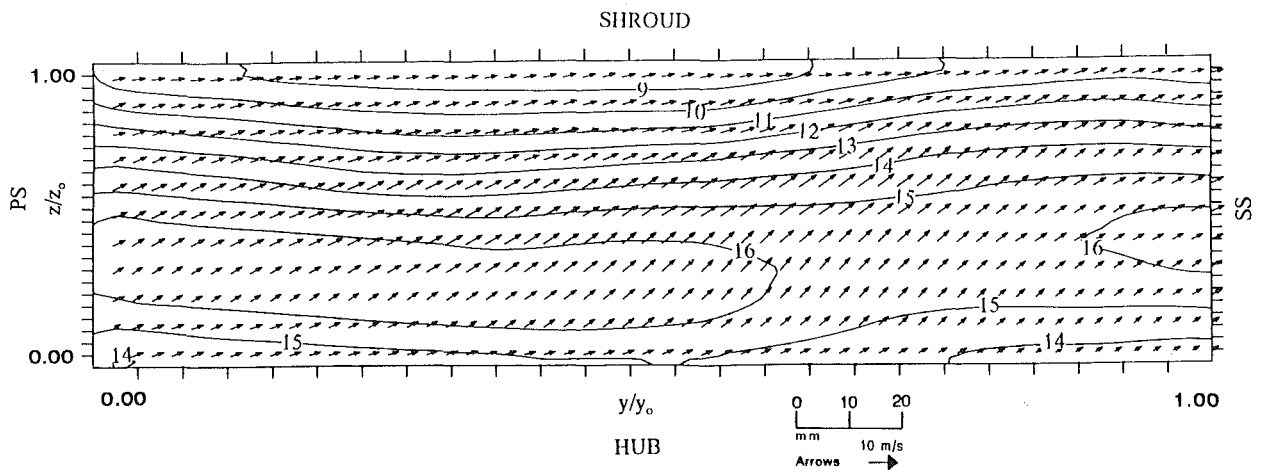


Fig. 8 Mean velocities at station 6 ($L/R_o = 0.33$)

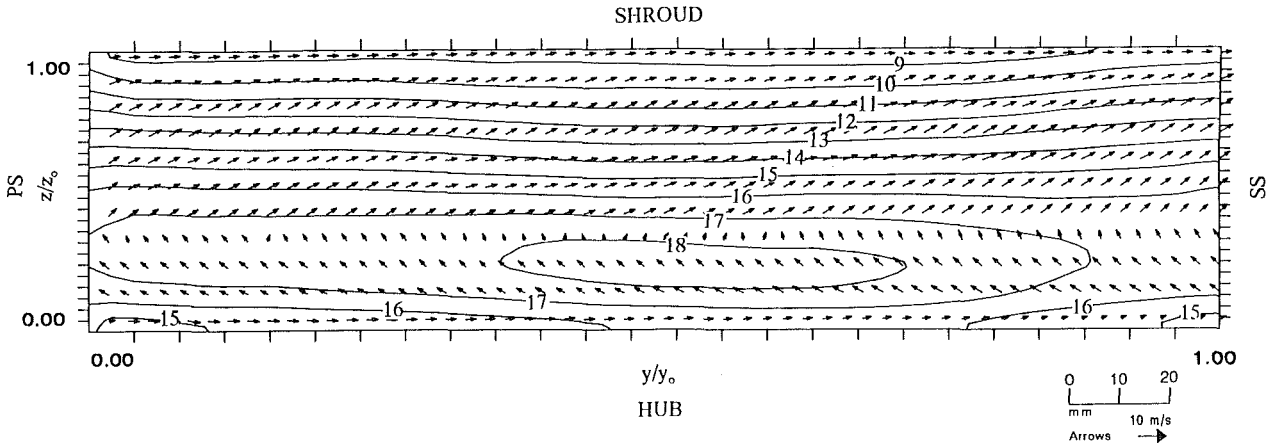


Fig. 9 Mean velocities at station 7 ($L/R_o = 0.39$)

orientation at fixed wind tunnel speed. The coefficients K and H were also obtained through a least rms error technique. The calibration procedure is similar to that detailed by Jøngensen (1971).

Phase lock loop circuitry was employed on the rig to generate a pulse every one third of a degree of rotation of the impeller to trigger the collection of the instantaneous hot-wire anemometer voltage through a 12 bit A/D converter connected to an 80286 microcomputer. On each revolution 57 readings were taken at 1/3 deg intervals to span the chosen impeller passage. These readings were recorded on each of 250 consecutive revolutions. This required a peak data acquisition rate of 9 kHz, which was achieved by means of 80286 machine code software. Between 11 and 13 axial measurement positions were used to complete the mesh of data points covering each measurement plane.

Downloaded 08 Mar 2011 to 193.140.144.9. Redistribution subject to ASME license or copyright; see http://www.asme.org/terms/Terms_Use.cfm

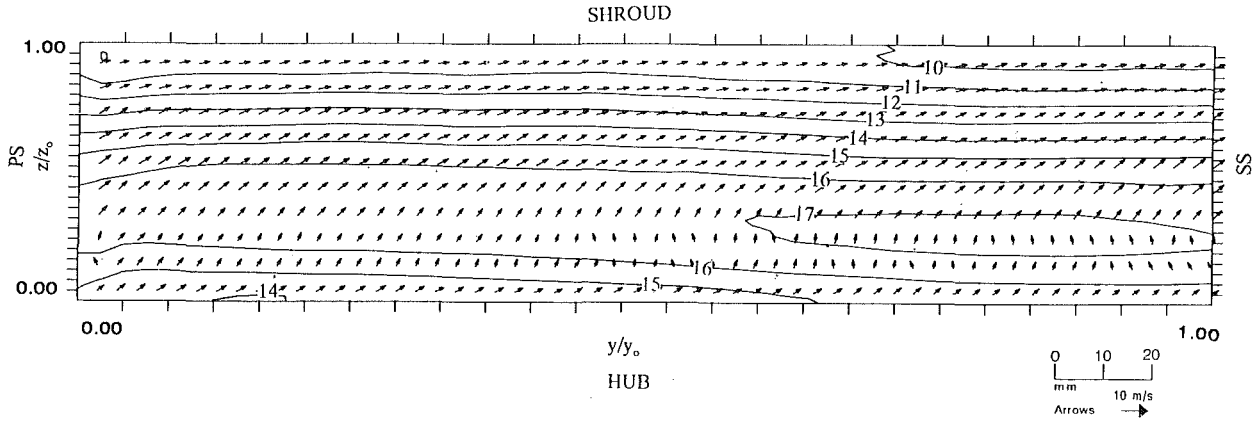


Fig. 10 Mean velocities at station 8 ($L/R_o = 0.45$)

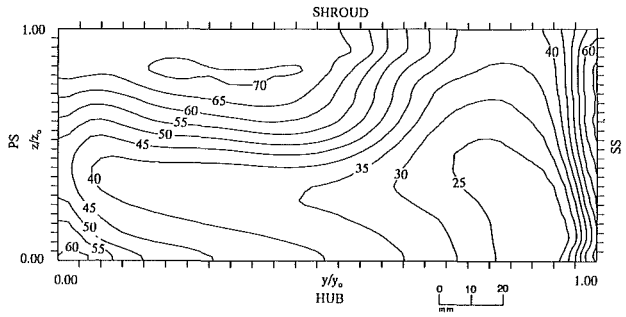


Fig. 11 Flow angle at station 1 ($L/R_o = 0.02$)

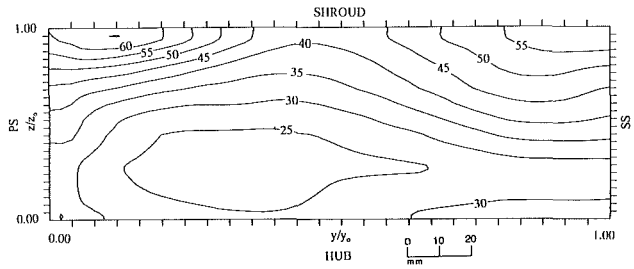


Fig. 14 Flow angle at station 4 ($L/R_o = 0.21$)

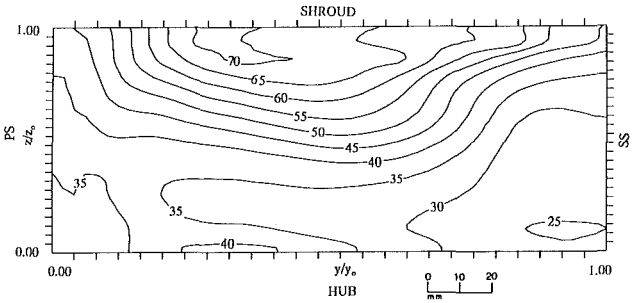


Fig. 12 Flow angle at station 2 ($L/R_o = 0.08$)

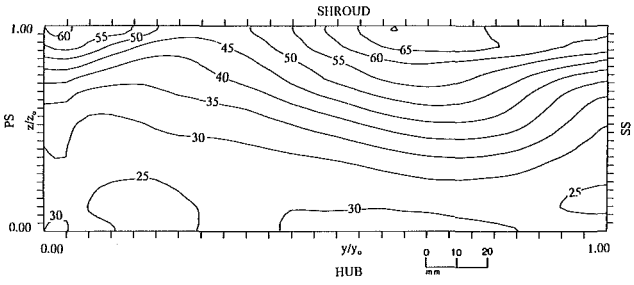


Fig. 13 Flow angle at station 3 ($L/R_o = 0.15$)

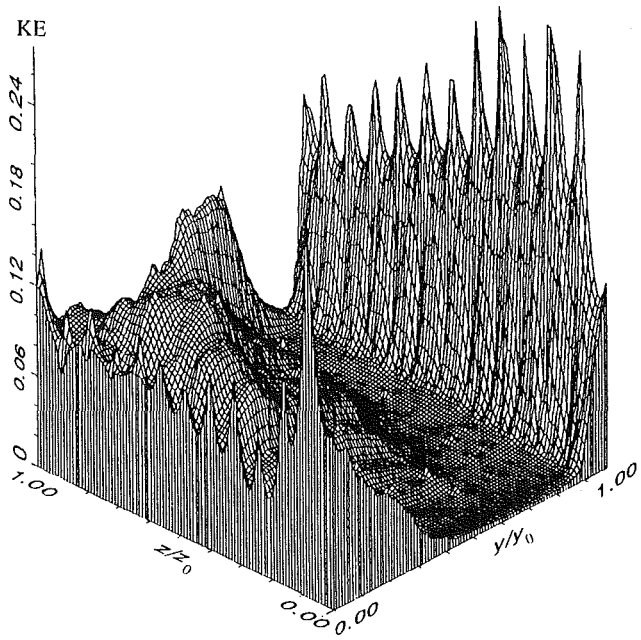


Fig. 15 Turbulent kinetic energy at station 1 ($L/R_o = 0.02$)

Analysis of Results. The 250 readings obtained for each measurement point on each of the three test runs were used to compute the tangential, radial, and axial velocity components and the turbulent kinetic energy using the King's law calibrations and the directional coefficients K and H.

As a check on the accuracy of the results, the flow rate was determined through numerical integration of the radial velocity component. The maximum deviation in flow rate between stations was found to be 4.8 percent from the mean.

Experimental Results

Mean Velocities. The mean velocities on the eight measurement planes in the diffuser are presented in Figs. 3–10. The radial velocity component is presented as a contour and the remaining velocity component in the measurement plane is shown as an arrow.

The flow pattern at Station 1 (Fig. 3), which is 12 mm downstream of the impeller, is similar to that observed at the last station within the impeller as reported by Farge and John-

Downloaded 08 Mar 2011 to 193.140.144.9. Redistribution subject to ASME license or copyright; see http://www.asme.org/terms/Terms_Use.cfm

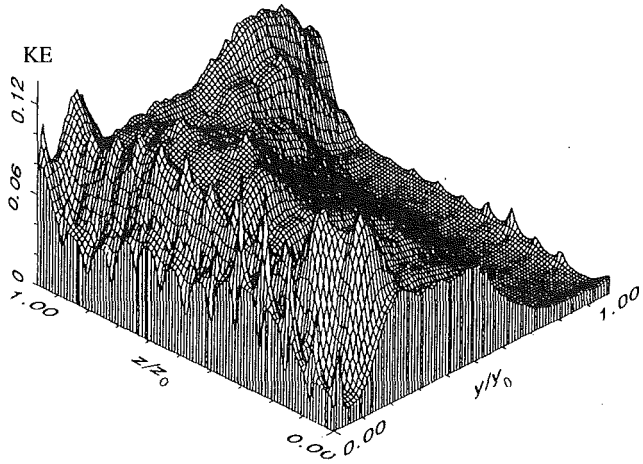


Fig. 16 Turbulent kinetic energy at station 2 ($L/R_o = 0.08$)

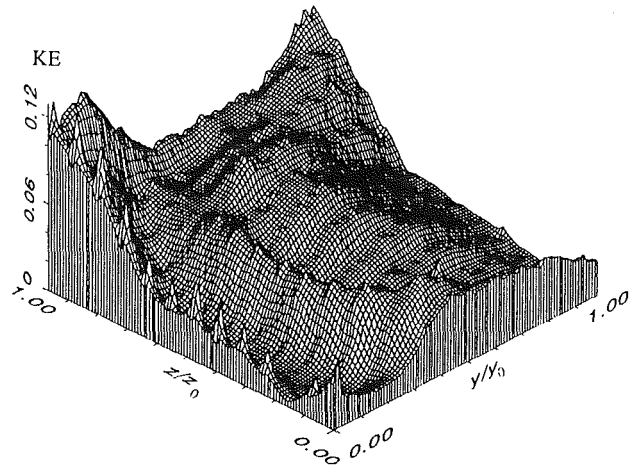


Fig. 17 Turbulent kinetic energy at station 3 ($L/R_o = 0.15$)

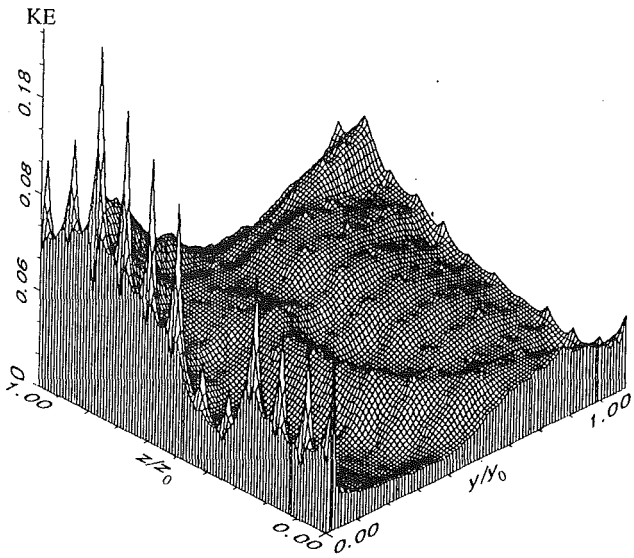


Fig. 18 Turbulent kinetic energy at station 4 ($L/R_o = 0.21$)

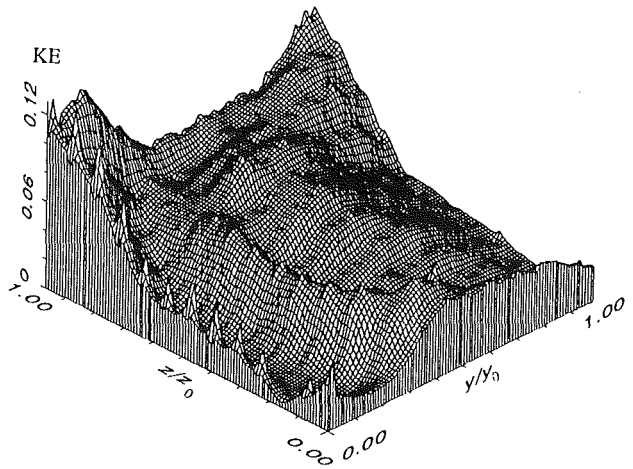


Fig. 19 Turbulent kinetic energy at station 5 ($L/R_o = 0.27$)

son (1990). Strong secondary flows in the impeller strip boundary layer fluid from the walls and carry it to the suction side shroud corner region where it accumulates in a passage wake. At the exit of the impeller this passage wake is located close to the center of the shroud wall and is moving toward the pressure side wall. In Fig. 3, the passage wake is on the shroud wall, and has moved close to the pressure side of the passage. Another feature of the impeller flow reported by Farge and Johnson (1990) and also by Krain (1988) in his backswept impeller is the presence of a strong anticlockwise passage vortex. This feature is also depicted in Fig. 3 as opposing axial flow vectors in the pressure side and suction side halves of the passage. The axial flow in the shroud to hub direction is particularly strong within the blade wake ($0.95 < y/y_o < 1$). In addition to these features observed in the impeller, a blade wake can also be seen on the right-hand side of the diagram. The velocity decreases by up to 53 percent within this wake. When the flow at station 2 (Fig. 4) is considered, it can be seen that the blade wake has been swept to the right by the strong tangential velocity component, such that the blade wake observed in Fig. 3 leaves the right-hand side of the diagram while the blade wake from the adjacent blade enters on the left-hand side. The deficit in velocity in the blade wake is also greatly diminished, indicating rapid mixing out in this region. This can be attributed to the strong opposed secondary velocity components that exist either side of the blade wake, which will greatly increase the shearing of the wake flow. The passage wake has been carried along the shroud by the tangential velocity, while altering little in size. However, the wake's shape has been modified as the low-energy fluid has spread farther along the shroud surface. Mixing out of the passage wake has not been significantly enhanced here by the interaction between the flow from neighboring passages; however, this is probably not the case in radial impellers running at below design flow rates where the passage wake is on the suction side blade surface at the impeller exit (see Johnson and Moore, 1983b). The strength of the passage vortex has diminished, which is primarily because the driving forces that produce secondary flow cease on exit from the impeller such that the passage vortex decays rapidly due to viscous dissipation.

At station 3 (Fig. 5), the blade wake is barely discernible at $y/y_o \cong 0.2$, but has continued to migrate in the pressure side to suction side direction. The passage wake has also continued to move in this same direction across the shroud. It is interesting to note that the wake moves in this direction more rapidly than the high-velocity jet (located at $y/y_o = 0.5$, $z/z_o = 0.3$). This is because the jet had a much higher relative tangential velocity than the wake in the impeller, which led to a lower absolute tangential velocity in the diffuser. The associated difference in flow angle ($\tan^{-1}(u_\theta/u_r)$) between jet and wake is marked (Figs. 11–14) and is of particular significance in the design of vaned diffusers where a compensatory variation in the vane angle across the span would be beneficial in minimizing flow separation. As the flow progresses through stations 4 to 8, variations in the blade to blade direction are gradually mixed out, and the passage wake eventually spreads out to cover the

Downloaded 08 Mar 2011 to 193.140.144.9. Redistribution subject to ASME license or copyright; see http://www.asme.org/terms/Terms_Use.cfm

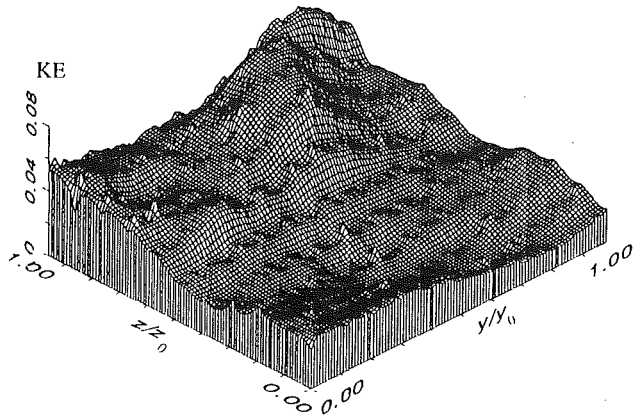


Fig. 20 Turbulent kinetic energy at station 6 ($L/R_o = 0.33$)

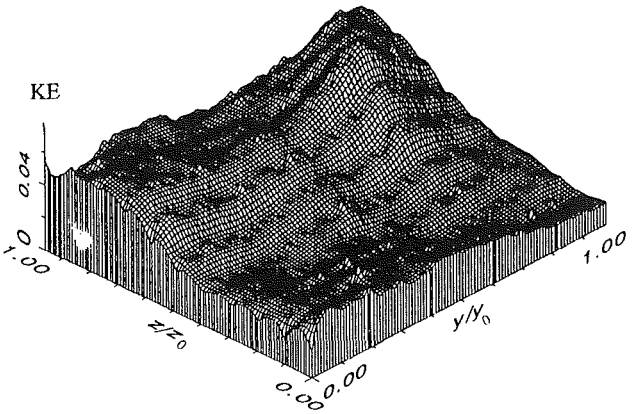


Fig. 21 Turbulent kinetic energy at station 7 ($L/R_o = 0.39$)

whole of the shroud surface fairly evenly. The hub wall boundary layer also develops slowly and although it is still thinner than the shroud boundary layer at station 8 (Fig. 10), the flow is tending toward a fully developed Couette flow between the two walls of the diffuser. A significant tangential velocity component still exists at station 8, but its magnitude is only some 30 percent of the value at station 1.

Turbulent Kinetic Energy. Distributions of turbulent kinetic energy are given in Figs. 15–22. The turbulent kinetic energy is defined as

$$\frac{\sqrt{u_\theta'^2 + u_r'^2 + u_z'^2}}{2.U_T} \tag{2}$$

where u_θ', u_r', u_z' are the tangential, radial, and axial rms fluctuating velocity components and U_T is the peripheral blade velocity at the impeller outlet.

High levels of turbulent kinetic energy occur not only in regions of mixing, but also in regions of unsteady flow where the fluctuations are of low frequency and do not result in significant Reynolds stresses. At station 1 (Fig. 15), similarly high levels of turbulent kinetic energy are observed in the blade and passage wakes. The rapid mixing out of the blade wake suggests that high Reynolds stresses are associated with the kinetic energy in the blade wake. However, in the passage wake the relatively slow mixing out rate suggests that only low Reynolds stress levels are present and the high levels of kinetic energy are due to low-frequency meandering of the wake position. This type of behavior has also been suggested by Hathaway et al. (1993) and is most likely due to low-frequency variations in flow rate, which will cause significant variations in wake position (Farge and Johnson, 1992). At station 2 (Fig. 16) the levels of kinetic energy are significantly decreased in the blade

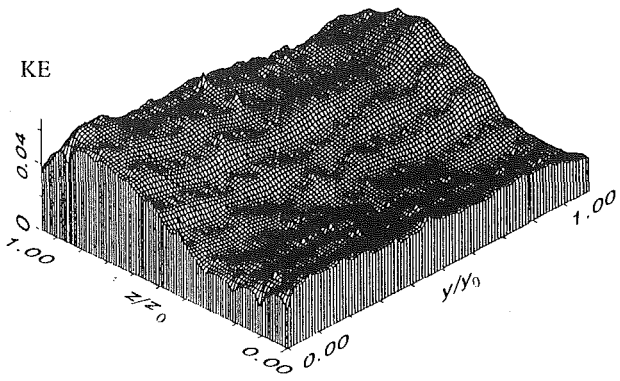


Fig. 22 Turbulent kinetic energy at station 8 ($L/R_o = 0.45$)

wake, which has now largely mixed out. The kinetic energy levels in the passage wake have only decreased a little from station 1 as might be expected as the wake has not significantly decreased in size. As the flow passes through the remaining stations (Figs. 17–22), the kinetic energy level in the passage wake decreases about threefold. The authors believe that this is not due to a significant decrease in the meandering of the wake in the tangential direction, but is due to the rapid decrease in the nonuniformities in this direction. This results in low fluctuating velocities as tangential movement of the passage wake does not result in significant variation in the velocity at any measurement point.

Conclusions

1 The flow entering the diffuser closely resembles that reported previously leaving the impeller. The most prominent features of the flow are a passage wake close to the center of the shroud wall and a strong anticlockwise passage vortex.

2 A strong blade wake is observed at station 1, but mixes out very rapidly because of the shearing effect of the opposed secondary flows either side of the wake. High levels of measured turbulent kinetic energy are associated with this process.

3 The passage wake mixes out only slowly. Although high levels of turbulent kinetic energy are observed within the passage wake, they are believed to result from low-frequency meandering of the wake position rather than high levels of Reynolds stress.

4 The passage vortex, characteristic of backswept centrifugal impeller flows, carries over to the diffuser, but decays fairly rapidly in the absence of the secondary flow mechanisms present in the impeller.

5 As the flow progresses through the impeller, variations in the tangential direction mix out, but variations in the axial direction tend to persist. The flow eventually resembles a Couette flow between the walls of the diffuser.

References

Eckardt, D., 1975, "Instantaneous Measurements in the Jet-Wake Discharge Flow of a Centrifugal Compressor Impeller," ASME *Journal of Engineering for Power*, Vol. 97, pp. 337–346.

Farge, T. Z., and Johnson, M. W., 1990, "The Effect of Backswept Blading on the Flow in a Centrifugal Compressor Impeller," ASME Paper No. 90-GT-231.

Farge, T. Z., and Johnson, M. W., 1992, "Effect of Flow Rate on Loss Mechanisms in a Backswept Centrifugal Impeller," *Int J. Heat Fluid Flow*, Vol. 13, No. 2, pp. 189–196.

Hathaway, M. D., Chriss, R. M., Wood, J. R., and Strazisar, A. J., 1993, "Experimental and Computational Investigation of the NASA Low-Speed Centrifugal Compressor Flow Field," ASME JOURNAL OF TURBOMACHINERY, Vol. 115, pp. 527–542.

Inoue, M., and Cumpsty, N. A., 1984, "Experimental Study of the Centrifugal Impeller Discharge Flow in Vaneless Diffusers," ASME *Journal of Engineering for Gas Turbines and Power*, Vol. 106, pp. 455–467.

Johnson, M. W., and Moore, J., 1980, "The Development of Wake Flow in a Centrifugal Compressor," ASME *Journal of Engineering for Power*, Vol. 102, pp. 383–390.

Downloaded 08 Mar 2011 to 193.140.144.9. Redistribution subject to ASME license or copyright; see http://www.asme.org/terms/Terms_Use.cfm

Johnson, M. W., and Moore, J., 1983a, "Secondary Flow and Mixing Losses in a Centrifugal Compressor Impeller," ASME *Journal of Engineering for Power*, Vol. 105, pp. 24–32.

Johnson, M. W., and Moore, J., 1983b, "Influence of Flow Rate on the Wake in a Centrifugal Impeller," ASME *Journal of Engineering for Power*, Vol. 105, pp. 33–39.

Jøngensen, F. E., 1971, "Directional Sensitivity of Wire and Fiber Film Probes," *DISA Information*, No. 11, pp. 31–37.

Krain, H., 1988, "Swirling Impeller Flow," ASME JOURNAL OF TURBOMACHINERY, Vol. 110, pp. 122–128.

Maksoud, T. M. A., and Johnson, M. W., 1987, "Stress Tensor Measurements Within the Vaneless Diffuser of a Centrifugal Compressor," *Proc. IMech E Conf.*, Paper No. C263/87.

Mounts, J. S., and Brasz, J. J., 1992, "Analysis of the Jet/Wake Mixing in a Vaneless Diffuser," ASME Paper No. 92-GT-418.

Downloaded 08 Mar 2011 to 193.140.144.9. Redistribution subject to ASME license or copyright; see http://www.asme.org/terms/Terms_Use.cfm